Serotonergic and dopaminergic neurons in the dorsal raphe are differentially altered in a mouse model for parkinsonism.

Laura Boi[1†], Yvonne Johansson[2†], Raffaella Tonini[3], Rosario Moratalla[4,5], Gilberto Fisone[1‡]*, Gilad Silberberg[1‡]*.

1 Department of Neuroscience, Karolinska Institutet, Stockholm 17177, Sweden.
2 Sainsbury Wellcome Centre for Neural Circuits and Behaviour, University College London, London, UK.
3 Neuromodulation of Cortical and Subcortical Circuits Laboratory, Istituto Italiano di Tecnologia, Genova, Italy.
4 Cajal Institute, Spanish National Research Council (CSIC), Madrid, Spain.
5 CIBERNED, Instituto de Salud Carlos III, Madrid, Spain.

† These authors contributed equally to this work
‡ These authors contributed equally to this work
* Corresponding author

Abstract

Parkinson's disease (PD) is characterized by motor impairments caused by degeneration of dopamine neurons in the substantia nigra pars compacta. In addition to these symptoms, PD patients often suffer from non-motor co-morbidities including sleep and psychiatric disturbances, which are thought to depend on concomitant alterations of serotonergic and noradrenergic transmission. A primary locus of serotonergic neurons is the dorsal raphe nucleus (DRN), providing brain-wide serotonergic input. Here, we identified electrophysiological and morphological parameters to classify serotonergic and dopaminergic neurons in the murine DRN under control conditions and in a PD model, following striatal injection of the catecholamine toxin, 6-hydroxydopamine (6-OHDA). Electrical and morphological properties of both neuronal populations were altered by 6-OHDA. In serotonergic neurons, most changes were reversed when 6-OHDA was injected in combination with desipramine, a noradrenaline reuptake inhibitor, protecting the noradrenergic terminals. Our results show that the depletion of both noradrenaline and dopamine in the 6-OHDA mouse model causes changes in the DRN neural circuitry.

Introduction

Parkinson's Disease (PD) is a frequent neurodegenerative disorder characterized by the progressive loss of dopaminergic (DA) neurons in the nigrostriatal pathway, leading to bradykinesia, tremor, rigidity, and postural instability [1, 2]. These cardinal motor symptoms are typically addressed by administration of dopaminergic drugs or by deep brain stimulation. PD patients also experience non-motor symptoms including sleep, affective, and cognitive dysfunctions often preceding the motor disabilities [3, 4]. These comorbidities are in large part refractory to current PD treatments and are thought to be caused by neurodegenerative processes occurring in concomitance to the loss of midbrain dopaminergic neurons. However, the pathology underlying non-motor symptoms remains poorly understood.

Post-mortem studies in PD patients provided first insights into the brain areas which might be involved in the etiology of non-motor dysfunctions in PD. Besides the profound degeneration of the substantia nigra pars compacta (SNc), these studies found cell loss and reduced neurotransmitter release in other monoaminergic brain regions, including the dorsal and median raphe nuclei (DRN and MRN, respectively), and the locus coeruleus (LC) [1, 5-8]. The DRN constitutes the main source of serotonin in the brain with serotonergic cells ($DRN^{5\text{-}HT}$) accounting for 30-50% of its neurons [9]. $DRN^{5\text{-}HT}$ neurons have been implicated in numerous neuropsychiatric diseases, rendering them a potential neural substrate for non-motor symptoms in PD. $DRN^{5\text{-}HT}$ neurons are also of central interest in PD research because of their bidirectional, monosynaptic connection with the striatum [10, 11]. In fact, several studies have shown that serotonergic markers and transmitter levels are altered in Parkinson patients as well as in non-human primate and rodent models of PD [12-19]. Notably, alterations in the serotonergic system have also been related to non-motor comorbidities in PD [20, 21]. Yet, functional investigations of $DRN^{5\text{-}HT}$ in rodent models of PD have led to conflicting results showing both increased and decreased activity in $DRN^{5\text{-}HT}$ neurons themselves as well as in their downstream targets [22-24]. Besides the serotonergic neurons, the DRN comprises other neuronal populations, including a small group (~1000 neurons in rats) of DA neurons (DRN^{DA})[25]. DRN^{DA} neurons have been linked to the regulation of pain, motivational processes, incentive memory, wakefulness and sleep-wake transitions [26-30], but their ultimate behavioral significance is yet to be elucidated [31-35]. DRN^{DA} neurons are directly innervated by dopaminergic neurons in the midbrain and have been found to show Lewy bodies in PD patients [6, 30, 36]. Yet, the physiology and pathophysiology of DRN^{DA} neurons in PD remains elusive. The sparsity of research on DRN^{DA} neurons is likely due to the technical challenges associated with targeting this population among the diverse cell types in the DRN and adjacent structures (e.g., retrorubral field, periaqueductal grey and LC), which often co-express signature genes, hampering their molecular identification and region-specific manipulations with cre driver lines [9, 36-39].

Recently, this issue has been addressed by Pinto and colleagues who showed that DRN^{DA} neurons are most faithfully labelled in transgenic mice in which the expression of cre is linked to the DA transporter (DAT-cre) [36]. Previously, the membrane properties of DRN^{DA} neurons have only been addressed in mice in which DRN^{DA} neurons were identified based on the expression of the transcription factor Pitx3 or the enzyme tyrosine hydroxylase (TH) [37]. In Pitx3-GFP mice, about 70% of GFP-positive neurons are TH-positive (TH+) as shown by immunohistochemistry. Moreover, 40% of TH+ neurons in the DRN are not labelled in these mice, suggesting that this line targets a subpopulation of DRN^{DA} neurons [37]. The widely used TH-cre reporter line has been found to show ectopic expression of cre in non-dopaminergic neurons, probably caused by a transient developmental expression of TH [40, 41]. In addition, the TH-cre line also labels noradrenergic neurons in the neighboring LC [40], which produces most of the noradrenaline (NA) in the brain and is involved in mood control, cognition, and sleep regulation [42]. The large overlap of functions ascribed to the LC and DRN is thought to result from the complex reciprocal synaptic connections between these two brain areas: notably, the LC provides noradrenergic input to the DRN [43, 44] while receiving input from $DRN^{5\text{-}HT}$ neurons [45-47].

Here, we used ex vivo whole-cell patch clamp recordings and morphological reconstructions to characterize the electrophysiological and morphological properties of DRN^{DA} and $DRN^{5\text{-}HT}$ neurons in wild type and DAT-tdTomato mice. Moreover, we studied the impact of catecholamine depletion on DRN^{DA} and $DRN^{5\text{-}HT}$ populations in the 6-OHDA toxin model of PD.

83 # Results

84 ## DRN^{DA} and $DRN^{5\text{-}HT}$ neurons are electrophysiologically distinct cell-types

85 To investigate the electrophysiological and morphological profile of DRN^{DA} neurons and to compare it to
86 $DRN^{5\text{-}HT}$ neurons, we performed whole-cell patch clamp recordings in coronal slices of adult wild type and
87 DAT-cre mice crossed with tdTomato reporter mice (Figure 1A). All neurons were filled with neurobiotin
88 and Alexa488 while recording. Alexa488 allowed us to take snapshots of recorded neurons at different time
89 points, thus facilitating the topographical registration of recorded neurons to the post-hoc stained slices
90 (Suppl. Figure 1). Using this approach, we obtained complete sets of electrophysiological and morphological
91 data from 75 neurons in the DRN. Cells were identified as $DRN^{5\text{-}HT}$ or DRN^{DA} neurons based on tryptophan
92 hydroxylase (TPH) or TH immunoreactivity, respectively (Figure 1A-D). In line with Fu et al. (2010)[38], none
93 of the recorded neurons was positive for both TPH and TH (n = 0/412). During the recordings, we used a
94 series of depolarizing and hyperpolarizing current steps and ramps that allowed us to characterize active
95 and passive membrane properties in detail (Figure 1E – G). Based on the electrophysiological data, we first
96 tested possible differences between TH+ neurons recorded in wild-type mice and tdTomato-positive
97 (tdTomato+) neurons recorded in DAT-tdTomato mice. We found no differences between these two groups
98 (n = 13 TH+ vs n = 30 tdTomato+ neurons, Suppl. Figure 2A) and neither within the subset of tdTomato+
99 neurons when comparing TH+ to TH-negative (TH-) neurons (n = 23 TH+ vs n = 6 TH- neurons, Suppl. Figure
100 2A–E). Since this small number of TH- neurons were positive for DAT and their electrophysiology
101 indistinguishable from TH+ DRN^{DA} neurons, the data was pooled. Please note that staining of recorded
102 neurons, i.e. immunohistochemistry on slices strained by hour-long patch-clamp recordings, is more
103 challenging as neurons can be lost after patching (no staining data) or the staining might be ambiguous.
104 Out of 114 tdTomato+ neurons only one cell displayed a different electrophysiological profile than all other
105 DRN^{DA} neurons, suggesting a false-positive rate of 0.8%. That neuron was TH- and displayed profoundly
106 distinct intrinsic properties, and was therefore excluded (Suppl. Figure 2F, G). Taken together, the
107 electrophysiological results support the use of the DAT-tdTomato mouse line when studying DRN^{DA} neurons
108 and data from both mouse lines were pooled. Recordings of DRN^{DA} neurons revealed distinctive
109 electrophysiological properties such as a slowly ramping membrane potential during constant current
110 injections giving rise to delayed spiking and postinhibitory hypoexcitability (Figure 1E). Moreover, most
111 DRN^{DA} neurons displayed rebound oscillations and sag currents (Figure 1E, F).

112 When comparing the electrophysiological properties of DRN^{DA} to $DRN^{5\text{-}HT}$ neurons, we observed numerous
113 differences between these two cell types, but here we focus on the five most significant ones. While $DRN^{5\text{-}HT}$
114 neurons spike with short delays in response to current steps and maintain a relatively constant action
115 potential (AP) amplitude, DRN^{DA} neurons display a longer delay to the first spike and the amplitude of
116 subsequent APs drops (Figure 1F-I). Additionally, the APs of $DRN^{5\text{-}HT}$ neurons rise faster, while their
117 afterhyperpolarization (AHP) is longer compared to DRN^{DA} neurons (Figure 1H, I). Lastly, the capacitance of
118 $DRN^{5\text{-}HT}$ neurons is significantly larger than in DRN^{DA} neurons (Figure 1I).

119 Next, we tested if DRN^{DA} neurons can be distinguished from $DRN^{5\text{-}HT}$ neurons based on these five
120 electrophysiological parameters. To this end, we standardized the data and ran a principal component
121 analysis (PCA) including all $DRN^{5\text{-}HT}$ neurons (i. e. all TPH-positive, TPH+), all TH+ neurons recorded in wild-
122 type mice and all tdTomato+ cells recorded in DAT-tdTomato mice (except for one outlier shown in Suppl.
123 Figure 2F, G). Plotting the first two principal components (PC) showed two separate clusters (Figure 1J,

124 insert). Unsupervised hierarchical cluster analysis based on PC1 and PC2 revealed the same two major
125 clusters and potential subclusters (Figure 1J). Mapping the molecular identity of the cells onto the
126 dendrogram revealed the separation of DRN^{5-HT} and DRN^{DA} neurons, while there was no branching
127 according to mouse line (wild type vs. DAT-tdTomato), further corroborating the validity of DAT-tdTomato
128 mice as a marker for DRN^{DA} neurons. Overall, these data suggest that electrophysiological parameters
129 themselves are sufficient to distinguish between DRN^{5-HT} and DRN^{DA} neurons.
130 In addition to DRN^{DA} and DRN^{5-HT} the DRN contains an unknown number of cell types and 47 out of 120
131 recorded neurons were neither TH+, nor TPH+ and did not express tdTomato. To test whether DRN^{DA} can
132 also be distinguished from those populations based on their electrophysiological profile, we ran a PCA on
133 20 standardized parameters and used the first three PCAs for unsupervised hierarchical clustering (Suppl.
134 Figure 3). Our analysis suggests that there might be four major electrophysiological cell types in the DRN.
135 In contrast to DRN^{DA} and DRN^{5-HT} neurons, a large proportion of the remaining cells showed rebound spiking
136 and biphasic AHPs, resembling the profiles of local interneurons in other brain areas (Suppl. Figure 3D, E).
137 Interestingly, the clustering also indicated that three TH- and tdTomato-negative (tdTomato-) neurons
138 belonged to the DRN^{DA} neurons and further analysis showed that they were indistinguishable from
139 molecularly identified DRN^{DA} neurons (Suppl. Figure 3C, F). These findings indicate that clustering can be
140 used to identify neurons that otherwise would have been excluded due to a lack of post-hoc staining data
141 or genetic driver lines.
142 Overall, our data show that DRN^{DA} neurons constitute an electrophysiologically distinct class of neurons in
143 the DRN expressing several hallmark properties, which are sufficient to identify them within the local DRN
144 circuitry.
145
146 **DRN^{DA} and DRN^{5-HT} neurons have different morphological properties**
147 Next, we characterized the morphological profile of DRN^{5-HT} and DRN^{DA} neurons. We focused on the analysis
148 of somatic and dendritic properties since a complete reconstruction of the axonal arborization could not
149 be retrieved from the slices. The analysis of the somatic properties showed that DRN^{5-HT} neurons had larger
150 cell bodies than DRN^{DA} neurons (Figure 2A, B), as measured in their area, perimeter, length, and width
151 (Figure 2B). Cell bodies also differed in shape, with DRN^{DA} neurons having more circular somata than DRN^{5-}
152 ^{HT} neurons, as indicated by the circularity index (Figure 2B). Analyzing the dendritic properties, we found
153 that DRN^{5-HT} neurons had four to five primary dendrites, compared to only two to three in DRN^{DA} neurons
154 (Figure 2A, C). Moreover, dendrites of DRN^{DA} neurons were frequently bipolar with the main primary
155 dendrites starting from opposite extremes of the soma. Both populations had relatively few bifurcations
156 (Figure 2C), but the DRN^{5-HT} neurons had significantly more terminations (Figure 2C). The overall dendritic
157 length did not differ between the DRN^{5-HT} and DRN^{DA} neurons: both populations had a mix of short and long
158 dendrites (Figure 2C). These data suggest that DRN^{5-HT} neurons have denser dendritic arborization than
159 DRN^{DA} neurons, mostly due to larger numbers of primary dendrites.
160 Altogether, our results show that DRN^{5-HT} and DRN^{DA} neurons have distinct morphological properties. DRN^{5-}
161 ^{HT} neurons are mostly multipolar neurons, with a big and complex soma and multiple primary dendrites,
162 while DRN^{DA} neurons have smaller and more circular cell bodies with bipolar dendrites.
163
164 **DA and NA depletion distinctly affect the membrane properties of DRN^{5-HT} neurons**

165 To elucidate how $DRN^{5\text{-}HT}$ and DRN^{DA} neurons might be affected in PD, we characterized these populations
166 in a mouse model of PD based on bilateral injection of the neurotoxin 6-OHDA in the dorsal striatum. This
167 approach leads to a partial lesion of catecholamine neurons, reproducing an early stage of parkinsonism in
168 which particularly non-motor symptoms such as depression- and anxiety-like behavior are manifested [48,
169 49]. In line with previous studies, we observed a 60-70% reduction of TH levels in the striatum (Suppl. Figure
170 4, [50]). Only mice meeting this criterion were included in the study. Measurement performed by ELISA
171 showed that the 6-OHDA injection did not alter the levels of 5-HT in the striatum (Suppl. Figure 4D), and
172 immunostaining showed that the striatal 6-OHDA injection did not cause degeneration of $DRN^{5\text{-}HT}$ or DRN^{DA}
173 neurons (Suppl. Figure 5).
174 Striatal injection of 6-OHDA has also been found to produce a partial loss of NA neurons in the LC [50] and
175 ELISA analysis showed that this approach induces approximately 60% loss of NA in the striatum (Suppl.
176 Figure 4E). In the present study, we determined the specific impact of NA dysfunction on the physiology of
177 $DRN^{5\text{-}HT}$ and DRN^{DA} neurons by pre-treating a group of mice with desipramine (DMI), a selective inhibitor of
178 NA reuptake, before injecting 6-OHDA (DMI+6-OHDA mice), which partially prevents striatal NA loss (Suppl.
179 Figure 4E). We then assessed the intrinsic properties of $DRN^{5\text{-}HT}$ and DRN^{DA} neurons in Sham-lesion (Sham),
180 6-OHDA- and DMI+6-OHDA-treated mice. Whole-cell recordings obtained from $DRN^{5\text{-}HT}$ neurons in control
181 mice revealed that 36% of $DRN^{5\text{-}HT}$ neurons were spontaneously active in slices and the proportion of
182 intrinsically active neurons was similar in mice injected with 6-OHDA (Sham: n = 12/33 $DRN^{5\text{-}HT}$ neurons, 6-
183 OHDA: n = 7/18 $DRN^{5\text{-}HT}$ neurons, Figure 3A). However, $DRN^{5\text{-}HT}$ neurons recorded in DMI+6-OHDA mice
184 showed an increased excitability: in this condition, 73% of $DRN^{5\text{-}HT}$ neurons were spontaneously active and
185 $DRN^{5\text{-}HT}$ neurons displayed lower rheobase currents than in control and 6-OHDA mice (Figure 3A, B). Since
186 the noradrenergic system is protected by DMI in these mice, these findings suggest that the 6-OHDA
187 induced lesion of midbrain dopaminergic neurons evoked the increased firing of $DRN^{5\text{-}HT}$ neurons.
188 While the excitability of $DRN^{5\text{-}HT}$ neurons was not affected in 6-OHDA mice, we observed that their firing
189 properties were profoundly altered: $DRN^{5\text{-}HT}$ neurons recorded in 6-OHDA mice displayed significantly
190 smaller and shorter APs and AHPs compared to Sham mice (Figure 3C-E). Moreover, $DRN^{5\text{-}HT}$ neurons fired
191 at higher frequencies and with shorter delays in response to current injections (Figure 3F-H). Finally, the
192 membrane time constant of $DRN^{5\text{-}HT}$ neurons was shorter in 6-OHDA injected mice than in Sham mice
193 (Figure 3I). Interestingly, these changes were not observed in 6-OHDA injected mice pre-treated with DMI,
194 suggesting that the noradrenergic lesion critically contributes to the changes in the firing properties of
195 $DRN^{5\text{-}HT}$ neurons in 6-OHDA mice. Taken together, these results indicate that $DRN^{5\text{-}HT}$ neurons are affected
196 in the 6-OHDA mouse model of PD. Specifically, lesions of the dopaminergic system increase the excitability
197 of $DRN^{5\text{-}HT}$ neurons whereas the combined lesion of the noradrenergic and dopaminergic systems changes
198 the firing properties of $DRN^{5\text{-}HT}$ neurons.
199
200 **Striatal DA depletion induces hypotrophy of $DRN^{5\text{-}HT}$ neurons**
201 Morphological analysis revealed a reduced soma size of the $DRN^{5\text{-}HT}$ neurons in 6-OHDA mice, which was
202 manifested as decreased area, perimeter, and major axes in comparison to control mice (Figure 4A-C).
203 Moreover, the increase in the circularity of the 6-OHDA group indicated that the shape of the soma of $DRN^{5\text{-}}$
204 ^{HT} neurons was also altered by the lesion (Figure 4C). These modifications were not observed in DMI + 6-
205 OHDA mice, suggesting that preserving the NA system protected the $DRN^{5\text{-}HT}$ neurons (Figure4A-C). Finally,
206 the injection of 6-OHDA also caused a significant reduction in the number of primary dendrites of $DRN^{5\text{-}HT}$

207 neurons in the 6-OHDA group and a tendency to fewer termination points (Figure 4D). The number of
208 bifurcations and the dendritic length were not affected by the lesion (Figure 4D). Globally, these results
209 suggest that the lesion produced by 6-OHDA induces a hypotrophic phenotype in $DRN^{5\text{-}HT}$ neurons
210 characterized by a shrinkage of the soma and a decrease in dendritic branching and that these alterations
211 are partly NA-dependent.
212
213 **Striatal DA depletion affects the firing of DRN^{DA} neurons independent of NA loss**
214 Finally, we assessed whether the striatal 6-OHDA lesion affects the physiology of DRN^{DA} neurons. Whole-
215 cell patch-clamp recordings revealed that 58% of DRN^{DA} neurons are spontaneously active in slices of Sham-
216 lesion mice (Figure 5A). In contrast, the proportion of intrinsically active neurons increased to 77% and 78%
217 of DRN^{DA} neurons in 6-OHDA injected mice with and without pre-treatment with DMI, respectively. In line
218 with this, silent DRN^{DA} neurons recorded in DMI + 6-OHDA mice were also found to have more depolarized
219 resting membrane potentials and hence to be closer to AP threshold (Figure 5B). Yet, active DRN^{DA} neurons
220 tended to fire at lower frequencies in all 6-OHDA mice compared to control mice.
221 In stark contrast to $DRN^{5\text{-}HT}$ neurons, the APs and AHPs of DRN^{DA} neurons were not affected in any 6-OHDA
222 mice (Figure 5C-E). In fact, we did not observe any change in the firing properties of DRN^{DA} neurons that
223 were dependent on the protection of the NA system with DMI (Figure 5). Like $DRN^{5\text{-}HT}$ neurons, DRN^{DA}
224 neurons displayed a reduction in spike latency in 6-OHDA mice, but the shortening of the delay was also
225 present in DMI+6-OHDA mice. Together, these results suggest that the electrophysiological properties of
226 DRN^{DA} neurons are affected in the 6-OHDA mouse model of PD and that these changes are primarily due
227 to the lesion of the nigrostriatal dopaminergic pathway.
228
229 **Striatal DA depletion increases soma complexity and dendritic branching in DRN^{DA} neurons**
230 The morphological analysis of DRN^{DA} neurons revealed that the striatal 6-OHDA injection caused a
231 significant reduction of the circularity from 0.82 (Sham) to 0.77 (6-OHDA) (Figure 6A-C), indicating
232 increased complexity of the DRN^{DA} soma. We also observed that this effect was not present in the mice
233 pre-treated with DMI (Figure 6C). The soma size was not affected by the lesion and no changes in the area,
234 perimeter, length, and width were found (Figure 6C). However, dendritic branching, as shown by the
235 increase in termination points and bifurcations in DRN^{DA} neurons was increased in 6-OHDA-injected mice,
236 but not in mice treated with a combination of DMI and 6-OHDA (Figure 6D). The number of primary
237 dendrites and the overall dendritic length were not affected by the 6-OHDA lesion (Figure 6D). Overall,
238 these data suggest that impairment of noradrenergic function caused by the striatal 6-OHDA injection
239 altered the soma shape and dendritic branching of DRN^{DA} neurons.
240
241 **Unilateral lesion of LC NA cells induces minor changes in DRN subpopulations**
242 Our results so far suggest that concomitant lesioning of the DA and NA system (6-OHDA model) has a severe
243 impact on $DRN^{5\text{-}HT}$ neurons which cannot be evoked when the NA system is partially protected (DMI + 6-
244 OHDA model). Therefore, we next assessed if selective lesioning of the NA system itself is sufficient to evoke
245 changes in electrical and morphological properties observed in $DRN^{5\text{-}HT}$ neurons recorded in 6-OHDA. To
246 that end we performed unilateral injections of 6-OHDA/saline in the LC (Suppl. Figure 6A), which lead to
247 approximately 50% loss of TH+ neurons in the LC (Suppl. Figure 6B, C). We chose to restrict the injection of
248 6-OHDA to one hemisphere because little is known about this type of lesion while the fundamental role of

249 the NA system in various neural processes is well established [51, 52]. We found that selective lesioning of
250 the LC ('6-OHDA-LC') did not alter the baseline activity levels, firing frequencies and resting membrane
251 potentials of DRN^{5-HT} and DRN^{DA} neurons (Suppl. Fig. 6D, E, K, L). However, DRN^{5-HT} neurons recorded in 6-
252 OHDA-LC had a lower input resistance at hyperpolarized membrane potentials, a shorter
253 afterhyperpolarization and a larger capacitance than DRN^{5-HT} neurons recorded in control mice (Sham-LC,
254 Suppl. Fig. 6E-G). Moreover, DRN^{DA} neurons recorded in 6-OHDA-LC showed a reduction in their sag
255 amplitudes (Suppl. Fig 6M, N). The other electrophysiological parameters were not significantly affected.
256 Morphological analysis revealed that the selective lesion of the noradrenergic system did not alter the size
257 and shape of cell bodies in either DRN subpopulation (Suppl. Figure 6H,I, O,P), however, the dendritic
258 branching of both subpopulations was altered, as shown by the increased length of primary dendrites in
259 DRN^{5-HT}neurons (Suppl. Figure 6J) and the increased number of primary dendrites in DRN^{DA} neurons (Suppl.
260 Figure 6Q).
261

262 ## Discussion

263 In the present study we combine *ex vivo* whole-cell patch clamp recordings with morphological
264 reconstructions and immunohistochemistry, to show that DRN^{DA} neurons have a distinct
265 electrophysiological profile, which is sufficient to distinguish them from DRN^{5-HT} neurons as well as other
266 neuron classes in the DRN. Utilizing this approach, we also reveal that, in a 6-OHDA mouse model of PD,
267 DRN^{5-HT} neurons display distinct pathophysiological changes depending on the loss of DA and NA. Notably,
268 degeneration of noradrenergic neurons affects not only the electrical properties of DRN^{5-HT} neurons but
269 also evokes hypotrophy of their cell bodies. In contrast, the loss of nigrostriatal DA mainly affects the
270 electrophysiological properties of DRN^{DA} neurons while concomitant loss of NA alters their morphology.
271
272 We used an extensive electrophysiological characterization protocol to quantify the differences between
273 the DRN^{DA} and DRN^{5-HT} populations. The electrophysiological properties agree with previous studies, such
274 as the spontaneous firing pattern seen in DRN^{DA} neurons [37], and the slow AHP of DRN^{5-HT} neurons [23].
275 Standard electrophysiological parameters were used to create a classification tool, which efficiently
276 identifies DRN^{5-HT} and DRN^{DA} cells, including DA neurons confirmed by TH staining and / or by fluorescent
277 expression in DAT-tomato mice (Figure 1). Importantly, the DRN^{DA} neurons recorded from wild-type and
278 DAT-tdTomato mice did not differ in their electrical properties, indicating that the transgene does not
279 interfere with the membrane properties of this population.
280
281 We showed that DRN^{DA} neurons share electrophysiological properties with other dopaminergic populations
282 in the midbrain such as postinhibitory hypoexcitability, rebound oscillations, a slowly ramping membrane
283 potential and sag currents [37, 53, 54], yet their electrophysiological profile is distinct from DRN^{5-HT} neurons
284 as well as other neuronal populations in the DRN. Most of the parameters extracted in our characterization
285 rely on intracellular recordings of the membrane potential. However, some properties such as spontaneous
286 firing and AP kinetics could be useful for *in vivo* characterization, even in extracellular recordings [55-57].
287 In addition to the DRN^{5-HT} and DRN^{DA} neuronal populations, a large fraction of neurons displayed
288 electrophysiological properties that were distinct from these two groups (Suppl. Figure 3), suggesting that
289 there are other neuronal subtypes in the DRN network, such as previously reported GABAergic,
290 glutamatergic, and peptidergic neurons [9, 10, 58-62].

291
292 In line with previous studies, the majority of DRN^{5-HT} neurons were large multipolar or fusiform neurons
293 with four to five primary dendrites, very distinct from the DRN^{DA} neurons [63-65]. Very little is known about
294 the morphology of the DRN^{DA} neurons, but previous studies identified small ovoid cells in the DRN which
295 are likely to correspond to the DRN^{DA} cells [37, 66]. Out of 25 reconstructed DRN^{5-HT} neurons, only one
296 displayed dendritic spines. Previous studies in rats described the presence of dendritic spines in most DRN^{5-HT}
297 neurons [67]. However, the study was performed in thicker slices and the dendritic spines were scarce
298 in the primary and secondary dendrites, while they became dense in the distal dendrites, thus it is possible
299 that in our study those dendrites were not present [67].
300
301 In the present study we assessed the impact on DRN cells of a striatal bilateral 6-OHDA lesion performed
302 with or without DMI pre-treatment, which has been shown to protect the NA neurons in the LC from the
303 6-OHDA-induced degeneration [50, 68, 69]. We found that both DRN^{5-HT} and DRN^{DA} populations were
304 affected in a cell-type specific manner by the combined action of 6-OHDA on DA and NA, with DRN^{5-HT}
305 neurons being particularly sensitive to changes in the noradrenergic system. Loss of SNc dopaminergic
306 neurons alone (6-OHDA + DMI) – which are known to target DRN^{5-HT} and DRN^{DA} neurons directly – increased
307 the excitability and spontaneous activity in DRN^{5-HT} neurons [10]. This is in line with previous *ex vivo* and *in*
308 *vivo* studies showing that the DRN^{5-HT} neurons display increased firing rates in rodents pre-treated with DMI
309 and injected with 6-OHDA [23, 70] As hypothesized by Prinz et al. [23], the selective loss of midbrain DA
310 may induce a homeostatic increase in the excitability of DRN^{5-HT} neurons. Our data contrast with a previous
311 *in vivo* study showing decreased firing activity in DRN^{5-HT} neurons where injection of 6-OHDA was preceded
312 by treatment with DMI and fluoxetine [24]. This dissimilarity may be related to species-specific (rat vs
313 mouse) and technical (intracerebroventricular vs striatal injections, recordings performed at 10 days vs
314 three weeks after the 6-OHDA injection). Importantly, in the same study identification of DRN^{5-HT} neurons
315 was not molecularly confirmed and the data may include other spontaneously active DRN neurons. In fact,
316 our recordings show that there are non-serotonergic neurons in the DRN, which are spontaneously active
317 and display a regular, slow firing frequency similar to DRN^{5-HT} neurons, highlighting the importance of
318 unequivocal identification of DRN cell types.
319
320 The present study shows that combined DA and NA lesioning affects DRN^{5-HT} neurons more profoundly than
321 selective loss of DA (Figure 3, 4). In mice treated with 6-OHDA only, several electrophysiological and
322 morphological properties were altered (Figure 3, 4). The time constant and AHP of DRN^{5-HT} neurons were
323 shorter and the neurons responded with higher firing frequencies to current injections than in Sham. This
324 finding suggests that the pronounced AHP and long tau of these neurons may act as a "brake" limiting their
325 maximum firing frequency in control conditions and that this brake is reduced when the NA system is
326 lesioned. Future studies are needed to assess if DRN^{5-HT} neurons in fact fire at higher rates in vivo in mice
327 treated with 6-OHDA. In contrast, such changes in DRN^{5-HT} neurons were prevented when the NA system
328 was protected by pre-treatment with DMI. These findings indicate an important role for NA as mediator of
329 changes in the activity and properties of DRN^{5-HT} neurons. The changes produced by the 6-OHDA lesion on
330 the DRN^{DA} population were less pronounced than and different from those in DRN^{5-HT} neurons. In terms of
331 electrophysiological properties, the observed changes were primarily in the DA only lesion (6-OHDA + DMI),
332 suggesting that unlike DRN^{5-HT}, DRN^{DA} neurons are affected by the loss of midbrain DA rather than the

accompanying changes in NA (Figure 5). Conversely, the morphological changes produced by 6-OHDA in DRN^{DA} neurons appeared to require a concomitant DA and NA lesion, suggesting a stronger impact of the NA modulation (Figure 6). Interestingly, unilateral lesions in the LC did not result in significant alterations in DRN neurons to the extent of the larger striatal lesions (Suppl. Figure 6). Although the trends of some of the electrophysiological parameters, such as the amplitude and duration of the AP and the AHP observed in $DRN^{5\text{-}HT}$ neurons, were similar to those induced by the 6-OHDA only lesion shown in Figure 3, the effects were smaller. This could be due to the more limited extent of the LC injections compared to the striatal ones as well as the unilateral LC vs. bilateral striatal lesioning. These two factors may have reduced the impact of NA depletion and should be further investigated in future studies.

Our results show that DRN neurons are affected by depletion of both DA and NA, thus raising the possibility that non-motor symptoms in PD are a result of the intricate organization of DA and NA neuromodulation as well as the interactions between the different DRN neuronal populations. Moreover, our results highlight the complex interplay in the DRN between NA, DA, and 5-HT, but the precise pathophysiological processes resulting from loss of NA, and specifically the impact on DRN, are yet to be elucidated.

In conclusion, our study provides a quantitative description and classification scheme for two major neuronal populations in the DRN, $DRN^{5\text{-}HT}$ and DRN^{DA} neurons. We identified novel electrophysiological and morphological changes in these populations in response to DA and NA depletion in the basal ganglia. Considering the involvement of DRN and LC in the development of non-motor comorbidities, this study provides useful insights to understand better how these areas are affected in the parkinsonian condition. Moreover, our data pave the way for future experiments to characterize these subpopulations in terms of receptor expression and synaptic connectivity to shed light on their functional roles particularly with regard to the wide variety of non-motor symptoms observed in PD.

Methods

Experimental model details

All animal procedures were performed in accordance with the national guidelines and approved by the local ethics committee of Stockholm, Stockholms Norra djurförsöksetiska nämnd, under ethical permits to G. F. (N12148/17, 14673-22) and G. S. (N2020/2022). All mice (N=43) were group-housed under a 12 hr light / dark schedule and given ad libitum access to food and water. Wild-type mice ('C57BL/6J', #000664, the Jackson laboratory) and DAT-cre (Stock #006660 the Jackson laboratory) mice crossed with homozygous tdTomato reporter mice ('Ai9', stock #007909, the Jackson laboratory) were used.

6-OHDA model

Three-months old, male and female C57BL/6J or DAT-tdTomato were deeply anesthetized with Isoflurane and mounted on a stereotaxic frame (Stoelting Europe, Dublin, Ireland). To achieve a partial striatal lesion, each mouse received a bilateral injection of 1.25 µl of 6-hydroxydopamine hydrochloride (6-OHDA, Sigma-Aldrich, 4µg/µl) or vehicle (0.9 % NaCl + Ascorbic Acid 0.02%) in the dorsolateral striatum, according to the following coordinates: anteroposterior +0.6 mm, mediolateral ± 2.2, dorsoventral -3.2 from Bregma, as previously described [48, 71]. One group of mice (referred to as DMI + 6-OHDA) was pre-treated with one injection of desipramine hydrochloride (DMI, Sigma-Aldrich, 25mg/kg i.p.) 30 minutes before the 6-OHDA infusion in order to protect the noradrenergic system [50].

For the LC lesion, mice received a unilateral injection of 1 µl of 6-OHDA (Sigma-Aldrich, 4µg/µl) or vehicle (0.9 % NaCl + Ascorbic Acid 0.02%) according to the following coordinates: anteroposterior –5.4 mm, mediolateral –0.9, dorsoventral -3.8 from Bregma.

Slice preparation and electrophysiology

Three weeks after the 6-OHDA/vehicle injection, mice were deeply anaesthetized with isoflurane and decapitated. The brain was quickly removed and immersed in ice-cold cutting solution containing 205 mM sucrose, 10 mM glucose, 25 mM NaHCO3, 2.5 mM KCl, 1.25 mM NaH2PO4, 0.5 mM CaCl2 and 7.5 mM MgCl2. In all experiments, the brain was divided into two parts: the striatum was dissected from the anterior section for Western Blot and the posterior part was used to prepare coronal brain slices (250 µm) with a Leica VT 1000S vibratome. Slices were incubated for 30-60 min at 34°C in a submerged chamber filled with artificial cerebrospinal fluid (ACSF) saturated with 95% oxygen and 5% carbon dioxide. ACSF was composed of 125 mM NaCl, 25 mM glucose, 25 mM NaHCO3, 2.5 mM KCl, 2 mM CaCl2, 1.25 mM NaH2PO4, and 1 mM MgCl2. Subsequently, slices were kept for at least 60 min at room temperature before recording. Whole-cell patch clamp recordings were obtained in oxygenated ACSF at 35°C. Neurons were visualized using infrared differential interference contrast (IR-DIC) microscopy (Zeiss FS Axioskop, Oberkochen, Germany). DAT-tdTomato positive cells were identified by switching to epifluorescence using a mercury lamp (X-cite, 120Q, Lumen Dynamics). Up to three cells were patched simultaneously. Borosilicate glass pipettes (Hilgenberg) of 6 - 8 MOhm resistance were pulled with a Flaming / Brown micropipette puller P-1000 (Sutter Instruments). The intracellular solution contained 130 mM K-gluconate, 5 mM KCl, 10 mM HEPES, 4 mM Mg-ATP, 0.3 mM GTP, 10 mM Na2-phosphocreatine (pH 7.25, osmolarity 285 mOsm), 0.2% neurobiotin (Vector laboratories, CA) and Alexa-488 (75 µM) was added to the intracellular solution

398 (Invitrogen). Recordings were made in current-clamp mode and the intrinsic properties of the neurons
399 were determined by a series of hyperpolarizing and depolarizing current steps and ramps, enabling the
400 extraction of sub- and suprathreshold properties. Recordings were amplified using MultiClamp 700B
401 amplifiers (Molecular Devices, CA, USA), filtered at 2kHz, digitized at 10-20kHz using ITC-18 (HEKA
402 Elektronik, Instrutech, NY, USA), and acquired using custom-made routines running on IgorPro
403 (Wavemetrics, OR, USA). Throughout all recordings pipette capacitance and access resistance were
404 compensated for and data were discarded when access resistance increased beyond 30 MOhm. Liquid
405 junction potential was not corrected for.
406
407 Quantification of electrophysiological parameters
408 Immediately after obtaining a whole-cell patch in DRN neurons, we first obtained a 10s voltage recording
409 of the neural activity without injecting any current. This recording was used to calculate the average resting
410 membrane potential in silent neurons and the firing frequency of spontaneously active neurons.
411 Subsequently, neurons were held at –60mV while an extensive series of de- and hyperpolarizing current
412 steps was applied. The amplitude of all current steps was scaled according to a test pulse that was set to
413 evoke one to two AP. The resulting voltage recordings were used to extract and calculate the following
414 parameters: The rheobase was defined as the minimum current required to evoke AP firing. AP parameters
415 were extracted from recordings where $DRN^{5\text{-}HT}$ neurons fired at 1 ± 0.3 Hz and DRN^{DA} neurons at 2 ± 0.3 Hz
416 (i.e. close to their average spontaneous firing frequency) and values from individual APs were averaged. AP
417 onset was extracted by quantifying where the rising slope of the AP (its first derivative) reached 5V/s and
418 the end of the AP was defined as the time where the AP had repolarized to the same membrane voltage as
419 found at the onset. The AP duration was calculated as the time between the onset and the offset. The
420 amplitude of the AP was defined as the voltage difference between the onset and its peak. The amplitude
421 of the AHP was defined as the voltage difference between the end of the AP and the subsequent local
422 minimum. The end of the AHP was found by using a sliding window of 50ms to assess when the slope of
423 the decaying AHP had first decreased to 0.005V/s or less. The AP drop rate was measured by injecting a
424 current ramp into the neurons that evoked multiple APs. The amplitude of these APs was extracted as
425 described above. The amplitude was plotted versus the injected current and a linear fit was applied whose
426 slope constitutes the AP drop rate. The delay to the first spike constitutes the time between the onset of
427 the current injection and the onset of the first AP in recordings. The input resistance was based on the
428 slope of a linear fit across all current–voltage steps that resulted in a steady state voltage between –90 and
429 –50mV (R = U / I). The steady state voltage was based on the average voltage found during a time window
430 starting 0.5s after the beginning of a 1s long current step and lasting until the end of the current step. The
431 amplitude of sag currents was defined as the average voltage difference between the steady state voltage
432 and the peak voltage evoked by current steps that hyperpolarized the neurons to –90 ± 5mV. The peak
433 voltage constituted the minimum voltage observed during the first 0.5s of the step. The time constant tau
434 was extracted following injection of a 5ms long hyperpolarizing current step. We applied an exponential fit
435 to the resulting voltage recording that started 1ms after the negative voltage peak had been reached and
436 ended when the membrane potential had returned to the average baseline voltage preceding the step. Tau
437 corresponds to K2 given the exponential fit is defined as y = K0 + K1*exp(-K2*x). Based on tau and the
438 steady-state input resistance, we calculated the capacitance C according to C = tau / resistance. The IF slope
439 was extracted from the linear fit applied to a current-frequency plot.

440

441 Immunofluorescence

442 Following the recordings, slices were fixated overnight at 4°C in a 4% paraformaldehyde solution. Slices
443 were then washed with PBS 1X. For the immunofluorescence, slices were treated with PBS 1X + Triton 0.3%
444 and then incubated with a blocking solution of Normal Serum 10% and Bovine Serum Albumin 1% for 1h at
445 room temperature. Afterward, slices were incubated overnight at 4°C with the following primary
446 antibodies: rabbit anti-TH (Millipore, 1:1000), mouse anti-TPH (Sigma Aldrich, 1:600) and Streptavidin
447 (Jackson Immunoresearch, 1:500). The following day, primary antibodies were washed out and slices were
448 incubated with the appropriate fluorochrome-conjugated secondary antibodies.
449 For the immunostainings in the striatum, SNc, LC and cell counting in DRN, mice were deeply anesthetized
450 and transcardially perfused with PFA 4%. The brains were extracted and post-fixed in PFA 4% for 24 hours.
451 40 µm coronal slices were prepared with a vibratome (Leica VT1000 S) and processed as described above.
452

453 Confocal Microscopy Analysis

454 The slices were imaged using Confocal (ZEISS LSM 800) at 10X and 40X and z-stacks were retrieved. For cell
455 identification, colocalization between neurobiotin and TH or TPH was evaluated.
456

457 Morphological analysis

458 For morphological analysis of dendrites, the confocal z-stacks were used in a semi-manual reconstruction
459 using neuTube [72] and custom code, as previously described [73]. Soma morphology was analyzed by
460 tracing manually the cell body profile, excluding dendritic trunks, in order to measure area (μm^2),
461 perimeter, major and minor axis length (µm) and circularity values. Circularity, calculated as the ratio
462 between the squared perimeter and the area (i.e. $perimeter^2/4\pi$ area), can be a value between 0 and 1 (1
463 for circular shapes and values < 1 for more complex shapes).
464 The morphological analysis was performed on the neurobiotin stacks.
465

466 Western Blot

467 The striata were sonicated in 1% sodium dodecyl sulfate and boiled for 10 min. Equal amounts of protein
468 (25 µg) for each sample were loaded onto 10% polyacrylamide gels and separated by electrophoresis and
469 transferred overnight to nitrocellulose membranes (Thermo Fisher, Stockholm, Sweden). The membranes
470 were immunoblotted with primary antibodies against actin (1:30,000, Sigma Aldrich, Stockholm, Sweden)
471 and TH (1:2000, Millipore, Darmstadt, Germany). Detection was based on fluorescent secondary antibody
472 binding (IR Dye 800CW and 680RD, Li-Cor, Lincoln, NE, USA) and quantified using a Li-Cor Odyssey infrared
473 fluorescent detection system (Li-Cor, Lincoln, NE, USA). The TH protein levels were normalized for the
474 corresponding actin detected in the sample and then expressed as a percentage of the control (Sham-
475 lesion).
476

477 Enzyme-linked immunosorbent assay

478 NA and 5-HT levels in the striatum were determined by Enzyme-linked immunosorbent assay (ELISA). Three
479 weeks after the 6-OHDA injection, mice were killed by decapitation and the striatum was dissected out
480 freehand on an ice-cold surface and weighted. The tissue was sonicated in a buffer with HCl 0.01M, EDTA
481 1mM and sodium metabisulfite 4 mM (25 µl/mg of tissue). The brain homogenates were centrifuged at 4

482 °C, 13000 rpm for 20 minutes and the supernatants were collected. The samples were assessed in analytic
483 duplicate using Noradrenaline and Serotonin Research ELISA kits (LDN, Germany), according to the
484 manufacturer's instructions. The absorbance at 450 nm was measured using a microplate reader. Tissue
485 concentrations of NA and 5-HT were determined using a standard curve.
486
487
488 Statistical Analysis
489 Statistical analysis of morphology data was performed using GraphPad Prism 9.2.0 and data were analyzed
490 by the Mann-Whitney U test, while data from WB and ELISA were analyzed by one-way ANOVA. Cell
491 counting data were analyzed by unpaired t-test. Electrophysiological data was first tested for normality
492 (Shapiro-Wilk test) before running an unpaired t-test for normally distributed data and the Mann-Whitney
493 U test for non-normally distributed data in matlab. Data are reported as average ± SEM. N indicates the
494 number of mice, while n indicates the number of cells. Significance was set at $p<0.05$.
495
496
497

Acknowledgments

We thank Elin Dahlberg for technical assistance and Kristoffer Tenebro Berglund for taking care of the mice. We also thank the members of the Silberberg and Fisone labs and the AND-PD consortium members for comments and discussions.

Funding

This work was supported by a Wallenberg Fellowship from the Knut & Alice Wallenberg Foundation (KAW 2017.0273), the Swedish Brain Foundation (Hjärnfonden, FO2021-0333), and the Swedish Medical Research Council (VR-M, 2019-0 1254) to GS, and a Swedish Research Council International Postdoc Grant (2020-06365) to YJ. RT, RA, GF, and GS are supported by an EU grant (H2020 848002 AND-PD).

Author contributions

Conceptualization: LB, YJ, RT, RM, GF, GS.
Investigation: YJ (electrophysiology, clustering analysis), LB (6-OHDA lesions, morphological analysis, cell counting, western blot, ELISA).
Visualization: YJ (electrophysiological and clustering results), LB (6-OHDA model, morphological reconstructions).
Supervision: GS and GF.
Writing—original draft: YJ and LB.
Writing—review & editing: LB, YJ, GF, GS.

Competing Interests

The authors declare that they have no competing interests.

Data availability

All raw data is available upon reasonable request.

524 # Figure Legends

525

526 **Figure 1. DRN^{DA} and $DRN^{5\text{-}HT}$ are electrophysiologically distinct cell-types. (A)** Scheme of the location of the DRN (pink)
527 in a coronal section (top) and at higher magnification together with two patch pipettes (center). Bottom: a
528 representative slice stained post recording for TPH, TH and neurobiotin revealing serotonergic neurons (arrows). The
529 ventricle is indicated with a dashed line. **(B)** Top: differential interference contrast (DIC) microscopy image (left) of
530 neurons that were filled with Alexa488 (right) and neurobiotin. Center, bottom: staining of the same neurons revealing
531 a TPH+ ($DRN^{5\text{-}HT}$) neuron and a TPH- and TH- cell. **(C)** Top: DIC image of recorded neurons that were filled with Alexa488
532 and neurobiotin. Center, bottom: staining of the same neurons revealing tdTomato- and TH+ (DRN^{DA}) neurons. **(D)**
533 Representative fluorescent (top), DIC (center) image and overlay (bottom) of a tdTomato+ neuron in a DAT-tdTomato
534 mouse. **(E)** Representative recordings depicting postinhibitory hypoexcitability, slowly ramping currents and rebound
535 oscillations in DRN^{DA} neurons. **(F)** Representative voltage responses to current injections in a TPH+ ($DRN^{5\text{-}HT}$) and TH+
536 (DRN^{DA}) neuron. **(G)** Ramping current injections reveal action potential (AP) amplitude accommodation. Gray circles
537 indicate the onset and peak of APs. **(H)** Amplitude and duration of the AP and AP afterhyperpolarization (AHP) in a
538 $DRN^{5\text{-}HT}$ and DRN^{DA} neurons. Gray circles indicate onset, peak, and end of the AP and AHP. **(I)** Quantification of
539 electrophysiological properties distinguishing $DRN^{5\text{-}HT}$ from DRN^{DA} neurons (AP drop rate: n = 32 $DRN^{5\text{-}HT}$, n = 43 DRN^{DA},
540 Capacitance: n = 32 $DRN^{5\text{-}HT}$, n = 43 DRN^{DA}, AP delay: n = 30 $DRN^{5\text{-}HT}$, n = 43 DRN^{DA}, AHP duration: n = 28 $DRN^{5\text{-}HT}$, n =
541 32 DRN^{DA}, N = 9; Wilcoxon Rank Sum Test). **(J)** Principal component analysis (PCA) of five electrophysiological
542 parameters (insert) and hierarchical cluster analysis based on PCA1 and PCA2 (Ward's method, Euclidean distance).
543 Intrinsic properties were sufficient to separate TPH+ cells (blue dash) from TH+ (red dash) cells. Bottom dashes
544 indicate wild type (black) and DAT-tdTomato (gray) mice. Data are shown as mean ± SEM, ***$p < 0.001$. Scale bars: A,
545 100 µm; B-D, 10 µm.

546

547 **Figure 2. DRN^{DA} and $DRN^{5\text{-}HT}$ have distinct morphological profiles. (A)** Top: representative digital reconstruction of a
548 $DRN^{5\text{-}HT}$. Bottom: representative digital reconstruction of a DRN^{DA}. **(B-F)** Morphological parameters describing the
549 soma size and shape of $DRN^{5\text{-}HT}$ and DRN^{DA} neurons ($DRN^{5\text{-}HT}$: n = 20, N = 3; DRN^{DA}: n = 27, N = 3; Mann-Whitney U
550 test). **(G-J)** Morphological parameters describing the dendritic tree of $DRN^{5\text{-}HT}$ and DRN^{DA} neurons ($DRN^{5\text{-}HT}$: n = 8, N =
551 3; DRN^{DA}: n = 7, N = 3; Mann-Whitney U test). Data are shown as mean ± SEM, ***$p < 0.001$. Scale bar: 10 µm.

552

553 **Figure 3. Lesions targeting primarily nigrostriatal dopamine increase the excitability of $DRN^{5\text{-}HT}$ neurons whereas loss**
554 **of NA affects their action potentials. (A)** Overview of workflow for analyzing the electrophysiological and
555 morphological properties of DRN neurons in Sham and 6-OHDA lesioned mice. **(B)** Top: pie charts showing the number
556 of spontaneously active (dark) and silent (pale) $DRN^{5\text{-}HT}$ neurons in three conditions: Sham (left), 6-OHDA-injected
557 mice (center) and 6-OHDA-injected mice pre-treated with desipramine (DMI + 6-OHDA, right). Bottom: representative
558 recordings of spontaneously active $DRN^{5\text{-}HT}$ neurons (I = 0 pA). **(C)** Quantification of the rheobase (left, Sham: n = 32,
559 6-OHDA: n = 17, DMI + 6-OHDA: n = 25), the firing frequency of spontaneously active cells (center, Sham: n = 11, 6-
560 OHDA: n = 6, DMI + 6-OHDA: n = 18), and the resting membrane potential of silent $DRN^{5\text{-}HT}$ neurons (right, Sham: n =
561 19, 6-OHDA: n = 11, DMI + 6-OHDA: n = 7). **(D)** Representative action potentials of $DRN^{5\text{-}HT}$ at low (left) and high (right)
562 temporal resolution. Gray circles indicate onset, offset, and peak of the APs as well as the end of the
563 afterhyperpolarization (AHP). **(E)** Quantification of the amplitude (left) and duration (right) of the APs of $DRN^{5\text{-}HT}$
564 neurons (Sham: n = 29, 6-OHDA: n = 16, DMI + 6-OHDA: n = 21). **(F)** Same as in (D) for the AHP. **(G)** Representative
565 responses of $DRN^{5\text{-}HT}$ neurons to current steps (I = +75 pA). **(H)** Quantification of firing frequency / injected current.
566 **(I)** Quantification of the delay to the first AP when injected with current eliciting 1Hz firing (Sham: n = 29, 6-OHDA: n
567 = 16, DMI + 6-OHDA: n = 21). **(J)** Quantification of the membrane time constant (tau) of $DRN^{5\text{-}HT}$ neurons (Sham: n =

32, 6-OHDA: n = 16, DMI + 6-OHDA: n = 21). Sham: N = 6 - 7; 6-OHDA: N = 7; DMI + 6-OHDA: N = 4; unpaired t-test or Mann-Whitney U test. Data are shown as mean ± SEM, * $p < 0.05$, ** $p < 0.01$.

Figure 4. Striatal injection of 6-OHDA induced a hypotrophic phenotype in the DRN$^{5\text{-}HT}$, which is prevented by pre-treatment with DMI. (A) Representative digital reconstructions of a DRN$^{5\text{-}HT}$ neuron in three different conditions: Sham (left), 6-OHDA-injected mice (center) and 6-OHDA-injected mice pre-treated with desipramine (right). **(B)** Representative confocal pictures of soma from DRN$^{5\text{-}HT}$ neurons in Sham (top), 6-OHDA-injected mice (center), and 6-OHDA-injected mice pre-treated with desipramine (bottom). **(C-G)** Morphological descriptors of the soma size and shape in DRN$^{5\text{-}HT}$ neurons (Sham: n = 20, N = 4; 6-OHDA: n = 19, N = 4; DMI + 6-OHDA: n = 17, N = 3; Mann-Whitney U test). **(H-K)** Morphological descriptors of the dendritic tree in DRN$^{5\text{-}HT}$ neurons (Sham: n = 8, N = 3, 6-OHDA: n = 6, N = 3: DMI + 6-OHDA: n = 6, N = 2; Mann-Whitney U test). Data are shown as mean ± SEM, ***$p<0.001$, **$p<0.01$. Scale bar: 10 µm.

Figure 5. Lesions targeting primarily SN dopamine depolarize DRN^{DA} neurons whereas concomitant loss of NA does not affect their action potentials. (A) Top: Pie charts showing the proportion of spontaneously active (dark) and silent (pale) DRN^{DA} neurons in three conditions: Sham (left), 6OHDA-injected mice (center) and 6-OHDA-injected mice pre-treated desipramine (DMI, right). Bottom: Representative recordings of spontaneously active DRN^{DA} (I = 0pA). **(B)** Quantification of the rheobase (left, Sham: n = 43, 6-OHDA: n = 31, DMI + 6-OHDA: n = 40), the firing frequency of spontaneously active (center, Sham: n = 25, 6-OHDA: n = 23, DMI + 6-OHDA: n = 31), and the resting membrane potential of silent DRN^{DA} neurons (right, Sham: n = 18, 6-OHDA: n = 7, DMI + 6-OHDA: n = 9). **(C)** Representative action potentials of DRN^{DA} at low (left) and high (right) temporal resolution. Gray circles indicate onset, offset, and peak of APs and the end of the afterhyperpolarization (AHP). **(D)** Quantification of the amplitude (left) and duration (right) of the APs of DRN^{DA} neurons (Sham: n = 34, 6-OHDA: n = 23, DMI + 6-OHDA: n = 35). **(E)** Same as in (D) for the AHP. **(F)** Representative responses of DRN^{DA} neurons to current steps (I = 75pA). Gray circles indicate the delay to the first AP. **(G-I)** Quantification of firing frequency / injected current (G, Sham: n = 31, 6-OHDA: n = 23, DMI + 6-OHDA: n = 27), the delay to the first AP when injected with current eliciting 2 Hz firing (H, Sham: n = 34, 6-OHDA: n = 23, DMI + 6-OHDA: n = 35), and the membrane time constant (I, Sham: n = 43, 6-OHDA: n = 29, DMI + 6-OHDA: n = 40) of DRN^{DA} neurons recorded (Sham: N = 8; 6-OHDA: N = 6; DMI + 6-OHDA: N = 6; unpaired t-test or Mann-Whitney U test). Data are shown as mean ± SEM, * $p < 0.05$.

Figure 6. Striatal injection of 6-OHDA increased soma complexity and branching in DRN^{DA}. (A) Representative digital reconstructions of a DRN^{DA} neuron in three different conditions: Sham (left), 6-OHDA-injected mice (center) and 6-OHDA-injected mice pre-treated with desipramine (right). **(B)** Representative confocal pictures of soma from DRN^{DA} neurons in Sham (top), 6-OHDA-injected mice (center), and 6-OHDA-injected mice pre-treated with DMI (bottom). **(C-G)** Morphological descriptors of the soma size and shape in DRN^{DA} neurons (Sham: n = 27, N = 7, 6-OHDA: n = 16, N = 4; DMI + 6-OHDA: n = 31, N = 5; Mann-Whitney U test). **(H-K)** Morphological descriptors of the dendritic tree in DRN^{DA} neurons. (Sham: n = 7, N = 3; 6-OHDA: n = 11, N = 4; DMI + 6-OHDA: n = 7, N = 3; Mann-Whitney U test). Data are shown as mean ± SEM, *$p<0.05$. Scale bar: 10 µm.

607 ## References
608

609 1. Braak, H., et al., *Staging of brain pathology related to sporadic Parkinson's disease.*
610 Neurobiol Aging, 2003. **24**(2): p. 197-211.
611 2. Jankovic, J., *Parkinson's disease: clinical features and diagnosis.* J Neurol Neurosurg
612 Psychiatry, 2008. **79**(4): p. 368-76.
613 3. Swick, T.J., *Parkinson's disease and sleep/wake disturbances.* Parkinsons Dis, 2012. **2012**:
614 p. 205471.
615 4. Chaudhuri, K.R. and A.H. Schapira, *Non-motor symptoms of Parkinson's disease:*
616 *dopaminergic pathophysiology and treatment.* Lancet Neurol, 2009. **8**(5): p. 464-74.
617 5. Halliday, G.M., et al., *Loss of brainstem serotonin- and substance P-containing neurons in*
618 *Parkinson's disease.* Brain Res, 1990. **510**(1): p. 104-7.
619 6. Halliday, G.M., et al., *Neuropathology of immunohistochemically identified brainstem*
620 *neurons in Parkinson's disease.* Ann Neurol, 1990. **27**(4): p. 373-85.
621 7. Gesi, M., et al., *The role of the locus coeruleus in the development of Parkinson's disease.*
622 Neurosci Biobehav Rev, 2000. **24**(6): p. 655-68.
623 8. Zarow, C., et al., *Neuronal loss is greater in the locus coeruleus than nucleus basalis and*
624 *substantia nigra in Alzheimer and Parkinson diseases.* Arch Neurol, 2003. **60**(3): p. 337-
625 41.
626 9. Huang, K.W., et al., *Molecular and anatomical organization of the dorsal raphe nucleus.*
627 Elife, 2019. **8**.
628 10. Pollak Dorocic, I., et al., *A whole-brain atlas of inputs to serotonergic neurons of the dorsal*
629 *and median raphe nuclei.* Neuron, 2014. **83**(3): p. 663-78.
630 11. Soghomonian, J.J., L. Descarries, and K.C. Watkins, *Serotonin innervation in adult rat*
631 *neostriatum. II. Ultrastructural features: a radioautographic and immunocytochemical*
632 *study.* Brain Res, 1989. **481**(1): p. 67-86.
633 12. Maillet, A., et al., *Serotonergic and Dopaminergic Lesions Underlying Parkinsonian*
634 *Neuropsychiatric Signs.* Mov Disord, 2021.
635 13. Jørgensen, L.M., et al., *Parkinson patients have a presynaptic serotonergic deficit: A*
636 *dynamic deep brain stimulation PET study.* J Cereb Blood Flow Metab, 2021. **41**(8): p.
637 1954-1963.
638 14. Cheshire, P., et al., *Serotonergic markers in Parkinson's disease and levodopa-induced*
639 *dyskinesias.* Mov Disord, 2015. **30**(6): p. 796-804.
640 15. Pifl, C., G. Schingnitz, and O. Hornykiewicz, *Effect of 1-methyl-4-phenyl-1,2,3,6-*
641 *tetrahydropyridine on the regional distribution of brain monoamines in the rhesus*
642 *monkey.* Neuroscience, 1991. **44**(3): p. 591-605.
643 16. Rylander, D., et al., *Maladaptive plasticity of serotonin axon terminals in levodopa-*
644 *induced dyskinesia.* Ann Neurol, 2010. **68**(5): p. 619-28.
645 17. Nayyar, T., et al., *Cortical serotonin and norepinephrine denervation in parkinsonism:*
646 *preferential loss of the beaded serotonin innervation.* Eur J Neurosci, 2009. **30**(2): p. 207-
647 16.
648 18. Taylor, T.N., et al., *Nonmotor symptoms of Parkinson's disease revealed in an animal*
649 *model with reduced monoamine storage capacity.* J Neurosci, 2009. **29**(25): p. 8103-13.

650 19. Karstaedt, P.J., et al., *Unilateral destruction of dopamine pathways increases ipsilateral*
651 *striatal serotonin turnover in rats.* Exp Neurol, 1994. **126**(1): p. 25-30.
652 20. Wilson, H., et al., *Serotonergic dysregulation is linked to sleep problems in Parkinson's*
653 *disease.* Neuroimage Clin, 2018. **18**: p. 630-637.
654 21. Politis, M., et al., *Depressive symptoms in PD correlate with higher 5-HTT binding in raphe*
655 *and limbic structures.* Neurology, 2010. **75**(21): p. 1920-7.
656 22. Kaya, A.H., et al., *Increased electrical and metabolic activity in the dorsal raphe nucleus of*
657 *Parkinsonian rats.* Brain Res, 2008. **1221**: p. 93-7.
658 23. Prinz, A., et al., *Increased excitability in serotonin neurons in the dorsal raphe nucleus in*
659 *the 6-OHDA mouse model of Parkinson's disease.* Exp Neurol, 2013. **248**: p. 236-45.
660 24. Guiard, B.P., et al., *Functional interactions between dopamine, serotonin and*
661 *norepinephrine neurons: an in-vivo electrophysiological study in rats with monoaminergic*
662 *lesions.* Int J Neuropsychopharmacol, 2008. **11**(5): p. 625-39.
663 25. Descarries, L., et al., *Dopaminergic projection from nucleus raphe dorsalis to neostriatum*
664 *in the rat.* J Comp Neurol, 1986. **249**(4): p. 511-20, 484-5.
665 26. Wenk, G.L., et al., *Behavioral, biochemical, histological, and electrophysiological effects*
666 *of 192 IgG-saporin injections into the basal forebrain of rats.* J Neurosci, 1994. **14**(10): p.
667 5986-95.
668 27. Lu, J., T.C. Jhou, and C.B. Saper, *Identification of wake-active dopaminergic neurons in the*
669 *ventral periaqueductal gray matter.* J Neurosci, 2006. **26**(1): p. 193-202.
670 28. Dzirasa, K., et al., *Dopaminergic control of sleep-wake states.* J Neurosci, 2006. **26**(41): p.
671 10577-89.
672 29. Cho, J.R., et al., *Dorsal Raphe Dopamine Neurons Modulate Arousal and Promote*
673 *Wakefulness by Salient Stimuli.* Neuron, 2017. **94**(6): p. 1205-1219.e8.
674 30. Lin, R., et al., *The Raphe Dopamine System Controls the Expression of Incentive Memory.*
675 Neuron, 2020. **106**(3): p. 498-514.e8.
676 31. Matthews, G.A., et al., *Dorsal Raphe Dopamine Neurons Represent the Experience of*
677 *Social Isolation.* Cell, 2016. **164**(4): p. 617-31.
678 32. Taylor, N.E., et al., *The Role of Glutamatergic and Dopaminergic Neurons in the*
679 *Periaqueductal Gray/Dorsal Raphe: Separating Analgesia and Anxiety.* eNeuro, 2019.
680 **6**(1).
681 33. Li, C., et al., *Mu Opioid Receptor Modulation of Dopamine Neurons in the Periaqueductal*
682 *Gray/Dorsal Raphe: A Role in Regulation of Pain.* Neuropsychopharmacology, 2016. **41**(8):
683 p. 2122-32.
684 34. Flores, J.A., et al., *Opiate anti-nociception is attenuated following lesion of large dopamine*
685 *neurons of the periaqueductal grey: critical role for D1 (not D2) dopamine receptors.* Pain,
686 2004. **110**(1-2): p. 205-14.
687 35. Flores, J.A., et al., *Role for dopamine neurons of the rostral linear nucleus and*
688 *periaqueductal gray in the rewarding and sensitizing properties of heroin.*
689 Neuropsychopharmacology, 2006. **31**(7): p. 1475-88.
690 36. Cardozo Pinto, D.F., et al., *Characterization of transgenic mouse models targeting*
691 *neuromodulatory systems reveals organizational principles of the dorsal raphe.* Nat
692 Commun, 2019. **10**(1): p. 4633.

693 37. Dougalis, A.G., et al., *Functional properties of dopamine neurons and co-expression of*
694 *vasoactive intestinal polypeptide in the dorsal raphe nucleus and ventro-lateral*
695 *periaqueductal grey.* Eur J Neurosci, 2012. **36**(10): p. 3322-3332.
696 38. Fu, W., et al., *Chemical neuroanatomy of the dorsal raphe nucleus and adjacent structures*
697 *of the mouse brain.* J Comp Neurol, 2010. **518**(17): p. 3464-94.
698 39. Okaty, B.W., et al., *Multi-Scale Molecular Deconstruction of the Serotonin Neuron System.*
699 Neuron, 2015. **88**(4): p. 774-91.
700 40. Lindeberg, J., et al., *Transgenic expression of Cre recombinase from the tyrosine*
701 *hydroxylase locus.* Genesis, 2004. **40**(2): p. 67-73.
702 41. Lammel, S., et al., *Diversity of transgenic mouse models for selective targeting of midbrain*
703 *dopamine neurons.* Neuron, 2015. **85**(2): p. 429-38.
704 42. Carter, M.E., et al., *Tuning arousal with optogenetic modulation of locus coeruleus*
705 *neurons.* Nat Neurosci, 2010. **13**(12): p. 1526-33.
706 43. Pudovkina, O.L., T.I. Cremers, and B.H. Westerink, *Regulation of the release of serotonin*
707 *in the dorsal raphe nucleus by alpha1 and alpha2 adrenoceptors.* Synapse, 2003. **50**(1): p.
708 77-82.
709 44. Trulson, M.E. and T. Crisp, *Role of norepinephrine in regulating the activity of serotonin-*
710 *containing dorsal raphe neurons.* Life Sci, 1984. **35**(5): p. 511-5.
711 45. Haddjeri, N., C. de Montigny, and P. Blier, *Modulation of the firing activity of*
712 *noradrenergic neurones in the rat locus coeruleus by the 5-hydroxtryptamine system.* Br J
713 Pharmacol, 1997. **120**(5): p. 865-75.
714 46. Singewald, N., et al., *Influence of excitatory amino acids on basal and sensory stimuli-*
715 *induced release of 5-HT in the locus coeruleus.* Br J Pharmacol, 1998. **123**(4): p. 746-52.
716 47. Aston-Jones, G., et al., *Serotonin selectively attenuates glutamate-evoked activation of*
717 *noradrenergic locus coeruleus neurons.* J Neurosci, 1991. **11**(3): p. 760-9.
718 48. Bonito-Oliva, A., D. Masini, and G. Fisone, *A mouse model of non-motor symptoms in*
719 *Parkinson's disease: focus on pharmacological interventions targeting affective*
720 *dysfunctions.* Front Behav Neurosci, 2014. **8**: p. 290.
721 49. Ztaou, S., et al., *Striatal cholinergic interneurons regulate cognitive and affective*
722 *dysfunction in partially dopamine-depleted mice.* Eur J Neurosci, 2018. **48**(9): p. 2988-
723 3004.
724 50. Bonito-Oliva, A., et al., *Cognitive impairment and dentate gyrus synaptic dysfunction in*
725 *experimental parkinsonism.* Biol Psychiatry, 2014. **75**(9): p. 701-10.
726 51. Poe, G.R., et al., *Locus coeruleus: a new look at the blue spot.* Nat Rev Neurosci, 2020.
727 **21**(11): p. 644-659.
728 52. Szot, P., et al., *Lesioning noradrenergic neurons of the locus coeruleus in C57Bl/6 mice*
729 *with unilateral 6-hydroxydopamine injection, to assess molecular, electrophysiological*
730 *and biochemical changes in noradrenergic signaling.* Neuroscience, 2012. **216**: p. 143-57.
731 53. Neuhoff, H., et al., *I(h) channels contribute to the different functional properties of*
732 *identified dopaminergic subpopulations in the midbrain.* J Neurosci, 2002. **22**(4): p. 1290-
733 302.
734 54. Lammel, S., et al., *Unique properties of mesoprefrontal neurons within a dual*
735 *mesocorticolimbic dopamine system.* Neuron, 2008. **57**(5): p. 760-73.

55. Strickland, J.A. and M.A. McDannald, *Brainstem networks construct threat probability and prediction error from neuronal building blocks.* Nat Commun, 2022. **13**(1): p. 6192.
56. Hajós, M., et al., *Neurochemical identification of stereotypic burst-firing neurons in the rat dorsal raphe nucleus using juxtacellular labelling methods.* Eur J Neurosci, 2007. **25**(1): p. 119-26.
57. Schweimer, J.V., et al., *Spike-timing relationship of neurochemically-identified dorsal raphe neurons during cortical slow oscillations.* Neuroscience, 2011. **196**(4): p. 115-23.
58. Dahlstroem, A. and K. Fuxe, *EVIDENCE FOR THE EXISTENCE OF MONOAMINE-CONTAINING NEURONS IN THE CENTRAL NERVOUS SYSTEM. I. DEMONSTRATION OF MONOAMINES IN THE CELL BODIES OF BRAIN STEM NEURONS.* Acta Physiol Scand Suppl, 1964: p. Suppl 232:1-55.
59. Weissbourd, B., et al., *Presynaptic partners of dorsal raphe serotonergic and GABAergic neurons.* Neuron, 2014. **83**(3): p. 645-62.
60. Gocho, Y., et al., *Electrophysiological and pharmacological properties of GABAergic cells in the dorsal raphe nucleus.* J Physiol Sci, 2013. **63**(2): p. 147-54.
61. Xu, Z., et al., *Whole-brain connectivity atlas of glutamatergic and GABAergic neurons in the mouse dorsal and median raphe nuclei.* Elife, 2021. **10**.
62. Bowker, R.M., et al., *Descending serotonergic, peptidergic and cholinergic pathways from the raphe nuclei: a multiple transmitter complex.* Brain Res, 1983. **288**(1-2): p. 33-48.
63. Rivera, H.M. and C.L. Bethea, *Ovarian steroids increase PSD-95 expression and dendritic spines in the dorsal raphe of ovariectomized macaques.* Synapse, 2013. **67**(12): p. 897-908.
64. Park, M.R., *Intracellular horseradish peroxidase labeling of rapidly firing dorsal raphe projection neurons.* Brain Res, 1987. **402**(1): p. 117-30.
65. Calizo, L.H., et al., *Raphe serotonin neurons are not homogenous: electrophysiological, morphological and neurochemical evidence.* Neuropharmacology, 2011. **61**(3): p. 524-43.
66. Diaz-Cintra, S., et al., *Nucleus raphe dorsalis: a morphometric Golgi study in rats of three age groups.* Brain Res, 1981. **207**(1): p. 1-16.
67. Li, Y.Q., et al., *Morphological features and electrophysiological properties of serotonergic and non-serotonergic projection neurons in the dorsal raphe nucleus. An intracellular recording and labeling study in rat brain slices.* Brain Res, 2001. **900**(1): p. 110-8.
68. Kamińska, K., et al., *Depressive-like neurochemical and behavioral markers of Parkinson's disease after 6-OHDA administered unilaterally to the rat medial forebrain bundle.* Pharmacol Rep, 2017. **69**(5): p. 985-994.
69. Fulceri, F., et al., *Nigrostriatal damage with 6-OHDA: validation of routinely applied procedures.* Ann N Y Acad Sci, 2006. **1074**: p. 344-8.
70. Wang, S., et al., *Unilateral lesion of the nigrostriatal pathway induces an increase of neuronal firing of the midbrain raphe nuclei 5-HT neurons and a decrease of their response to 5-HT(1A) receptor stimulation in the rat.* Neuroscience, 2009. **159**(2): p. 850-61.
71. Masini, D., et al., *A Guide to the Generation of a 6-Hydroxydopamine Mouse Model of Parkinson's Disease for the Study of Non-Motor Symptoms.* Biomedicines, 2021. **9**(6).
72. Feng, L., T. Zhao, and J. Kim, *neuTube 1.0: A New Design for Efficient Neuron Reconstruction Software Based on the SWC Format.* eNeuro, 2015. **2**(1).

73. Hjorth, J.J.J., et al., *The microcircuits of striatum in silico.* Proc Natl Acad Sci U S A, 2020. **117**(17): p. 9554-9565.

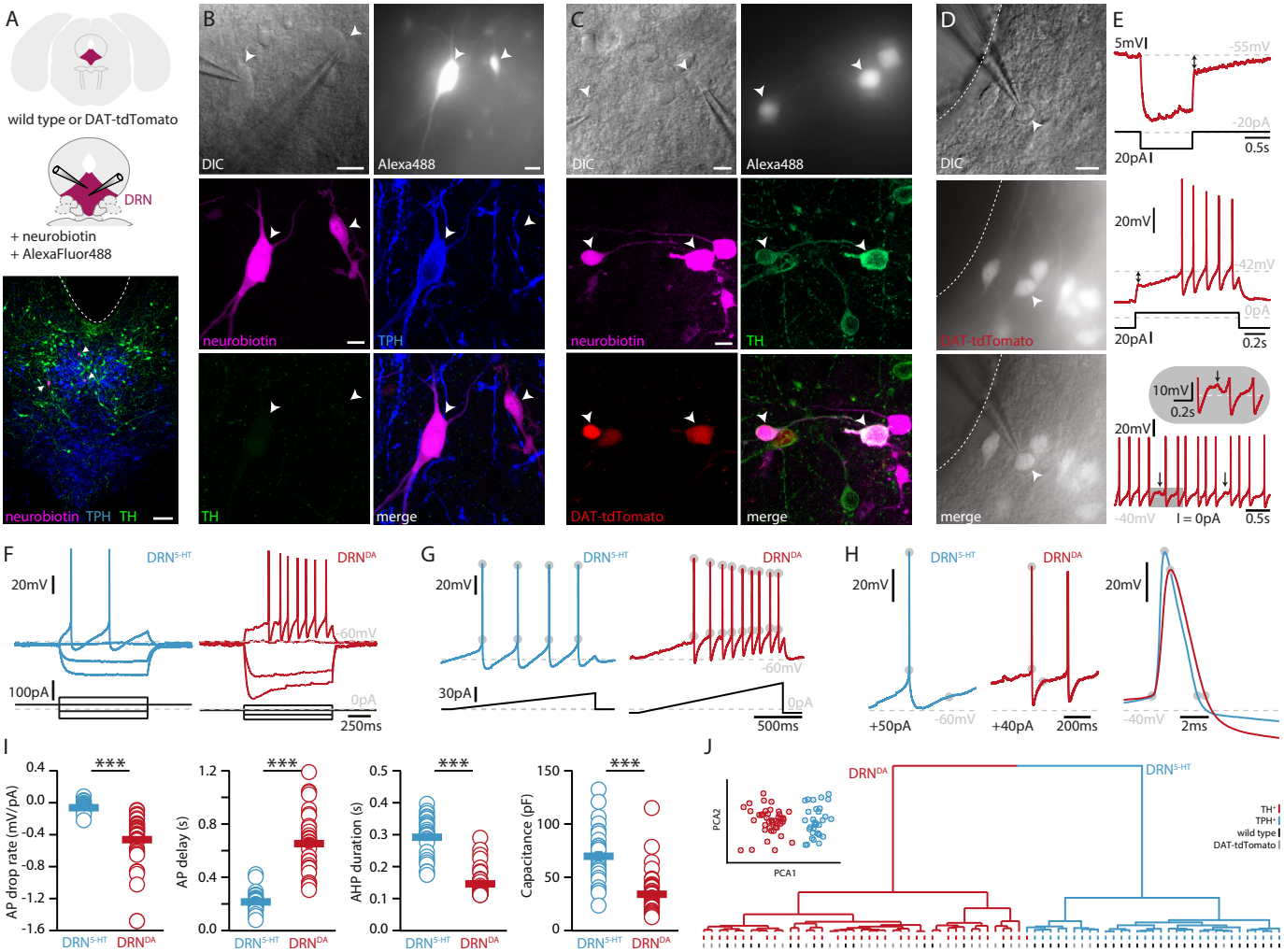
A
wild type or DAT-tdTomato
DRN
+ neurobiotin
+ AlexaFluor488
neurobiotin TPH TH
B
DIC
Alexa488
neurobiotin
TPH
TH
merge
C
DIC
Alexa488
neurobiotin
TH
DAT-tdTomato
merge
D
DIC
DAT-tdTomato
merge
E
5mV
-55mV
-20pA
20pA
0.5s
20mV
-42mV
0pA
20pA
0.2s
10mV
0.2s
20mV
-40mV
I = 0pA
0.5s
F
DRN5-HT
DRNDA
20mV
100pA
-60mV
0pA
250ms
G
DRN5-HT
DRNDA
20mV
30pA
-60mV
0pA
500ms
H
DRN5-HT
DRNDA
20mV
+50pA
-60mV
+40pA
200ms
-40mV
2ms
I
AP drop rate (mV/pA)
AP delay (s)
AHP duration (s)
Capacitance (pF)
***
DRN5-HT
DRNDA
J
DRNDA
DRN5-HT
PCA2
PCA1
TH+
TPH+
wild type
DAT-tdTomato

Fig. 1

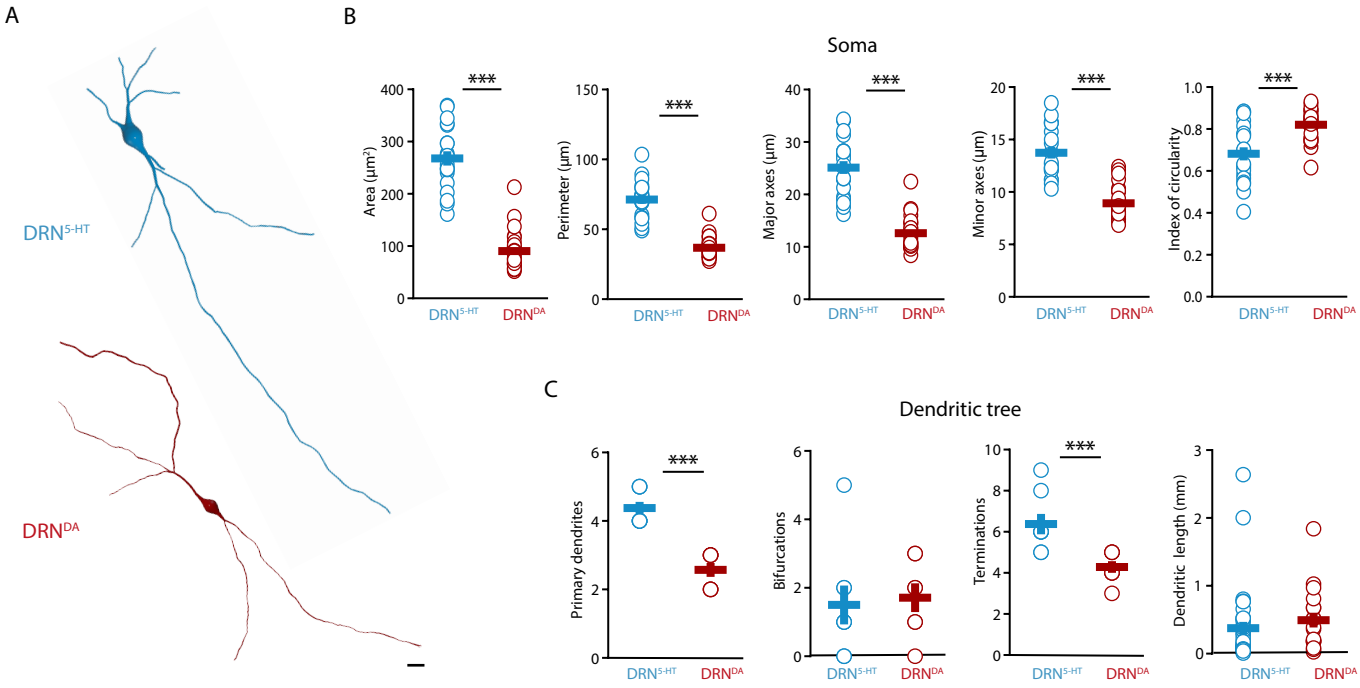
A
DRN5-HT
DRNDA
B
Soma
Area (µm²)
Perimeter (µm)
Major axes (µm)
Minor axes (µm)
Index of circularity
***
DRN5-HT
DRNDA
C
Dendritic tree
Primary dendrites
Bifurcations
Terminations
Dendritic length (mm)

Fig. 2

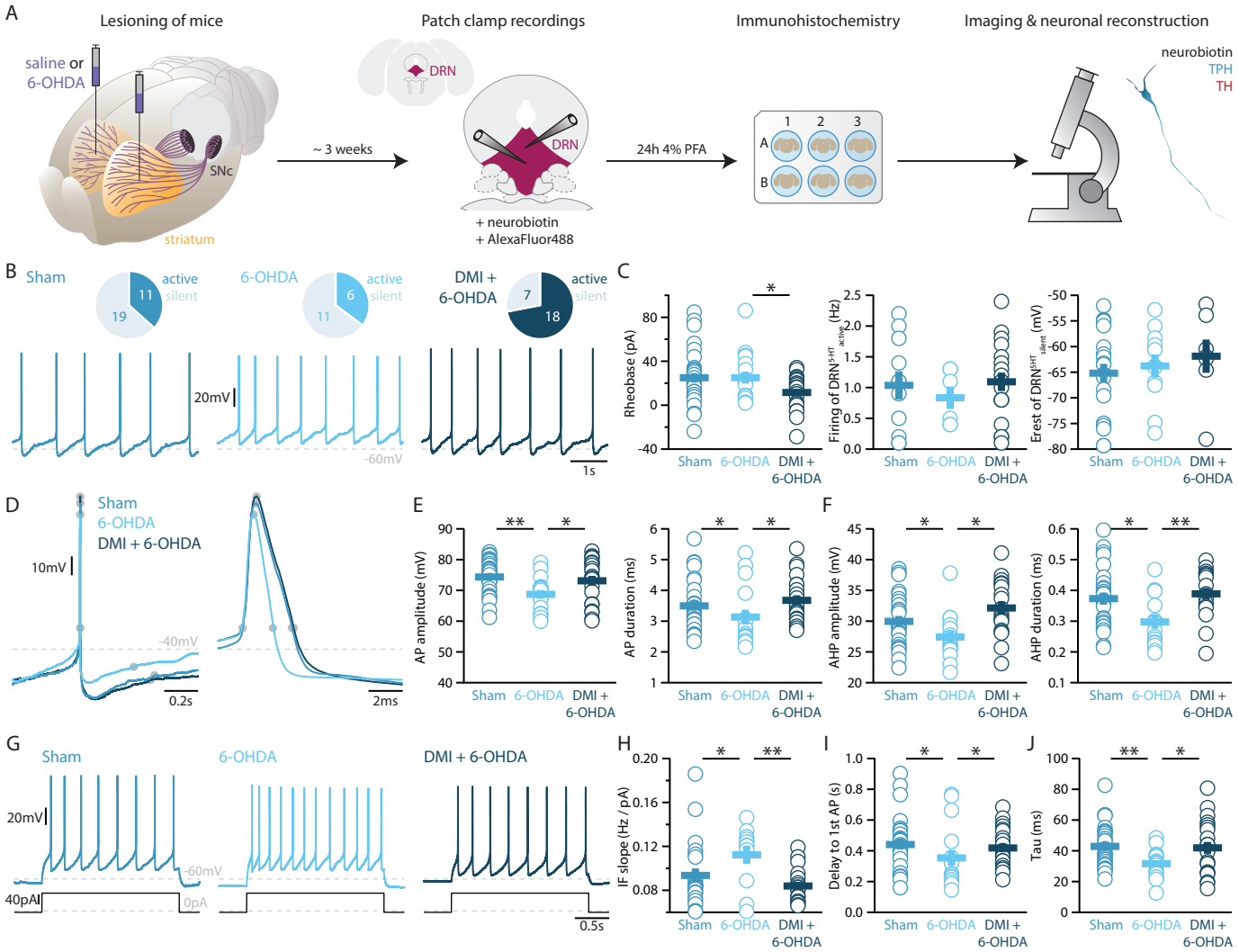
A
Lesioning of mice
Patch clamp recordings
Immunohistochemistry
Imaging & neuronal reconstruction
saline or
6-OHDA
SNc
striatum
~ 3 weeks
DRN
+ neurobiotin
+ AlexaFluor488
24h 4% PFA
neurobiotin
TPH
TH
B
Sham
6-OHDA
DMI +
6-OHDA
active
silent
20mV
-60mV
1s
C
Rheobase (pA)
Firing of DRN5-HT active (Hz)
Erest of DRN5-HT silent (mV)
Sham
6-OHDA
DMI +
6-OHDA
D
10mV
-40mV
0.2s
2ms
E
AP amplitude (mV)
AP duration (ms)
F
AHP amplitude (mV)
AHP duration (ms)
G
20mV
40pA
0pA
0.5s
H
IF slope (Hz / pA)
I
Delay to 1st AP (s)
J
Tau (ms)

Fig. 3

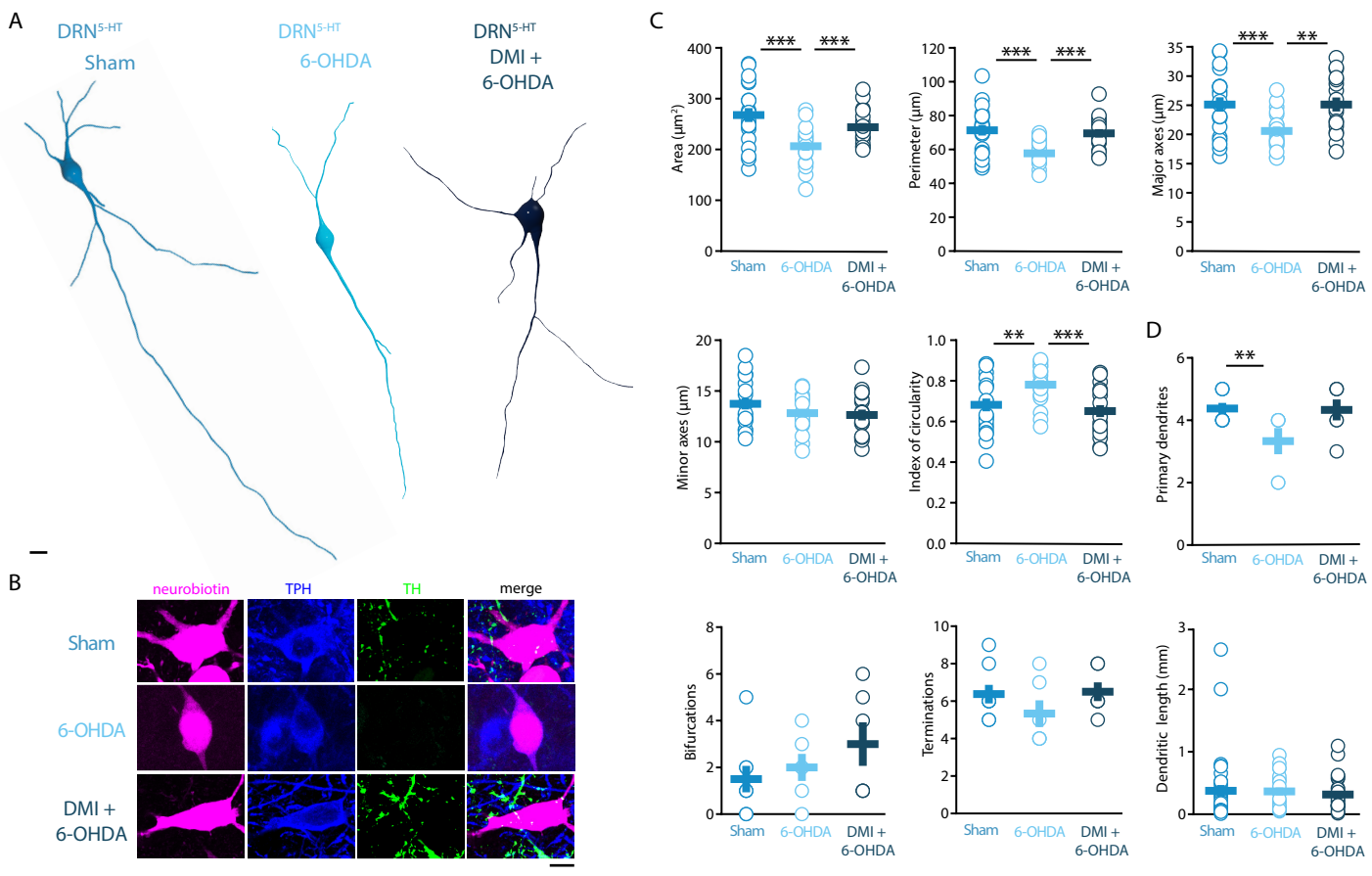
A
DRN5-HT
Sham
DRN5-HT
6-OHDA
DRN5-HT
DMI +
6-OHDA
B
neurobiotin
TPH
TH
merge
Sham
6-OHDA
DMI +
6-OHDA
C
Area (μm²)
Perimeter (μm)
Major axes (μm)
Minor axes (μm)
Index of circularity
Bifurcations
Terminations
Dendritic length (mm)
Sham
6-OHDA
DMI +
6-OHDA
D
Primary dendrites

Fig. 4

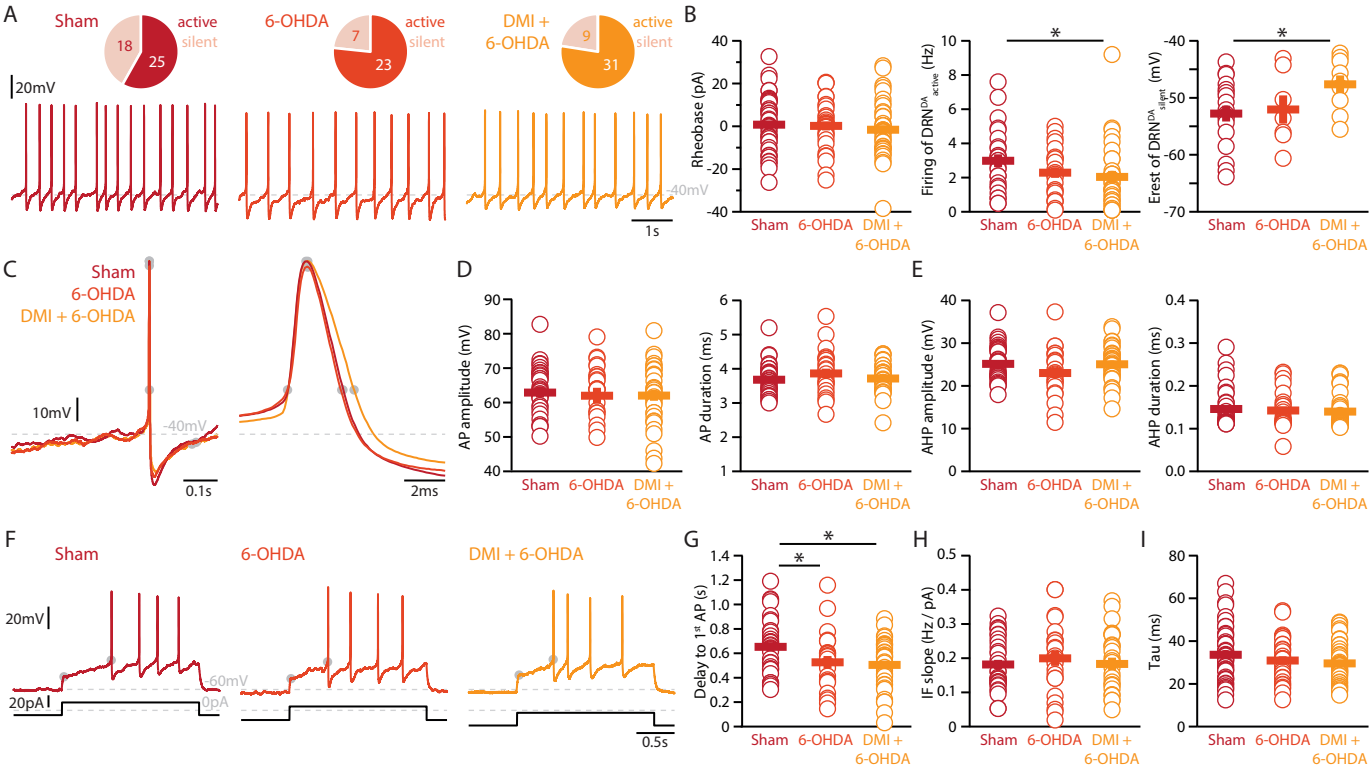
A
Sham
active
silent
18
25
6-OHDA
7
23
DMI + 6-OHDA
9
31
20mV
-40mV
1s
B
Rheobase (pA)
Firing of DRN$^{DA}_{active}$ (Hz)
Erest of DRN$^{DA}_{silent}$ (mV)
Sham
6-OHDA
DMI + 6-OHDA
C
Sham
6-OHDA
DMI + 6-OHDA
10mV
-40mV
0.1s
2ms
D
AP amplitude (mV)
AP duration (ms)
E
AHP amplitude (mV)
AHP duration (ms)
F
Sham
6-OHDA
DMI + 6-OHDA
20mV
-60mV
20pA
0pA
0.5s
G
Delay to 1st AP (s)
H
IF slope (Hz / pA)
I
Tau (ms)

Fig. 5

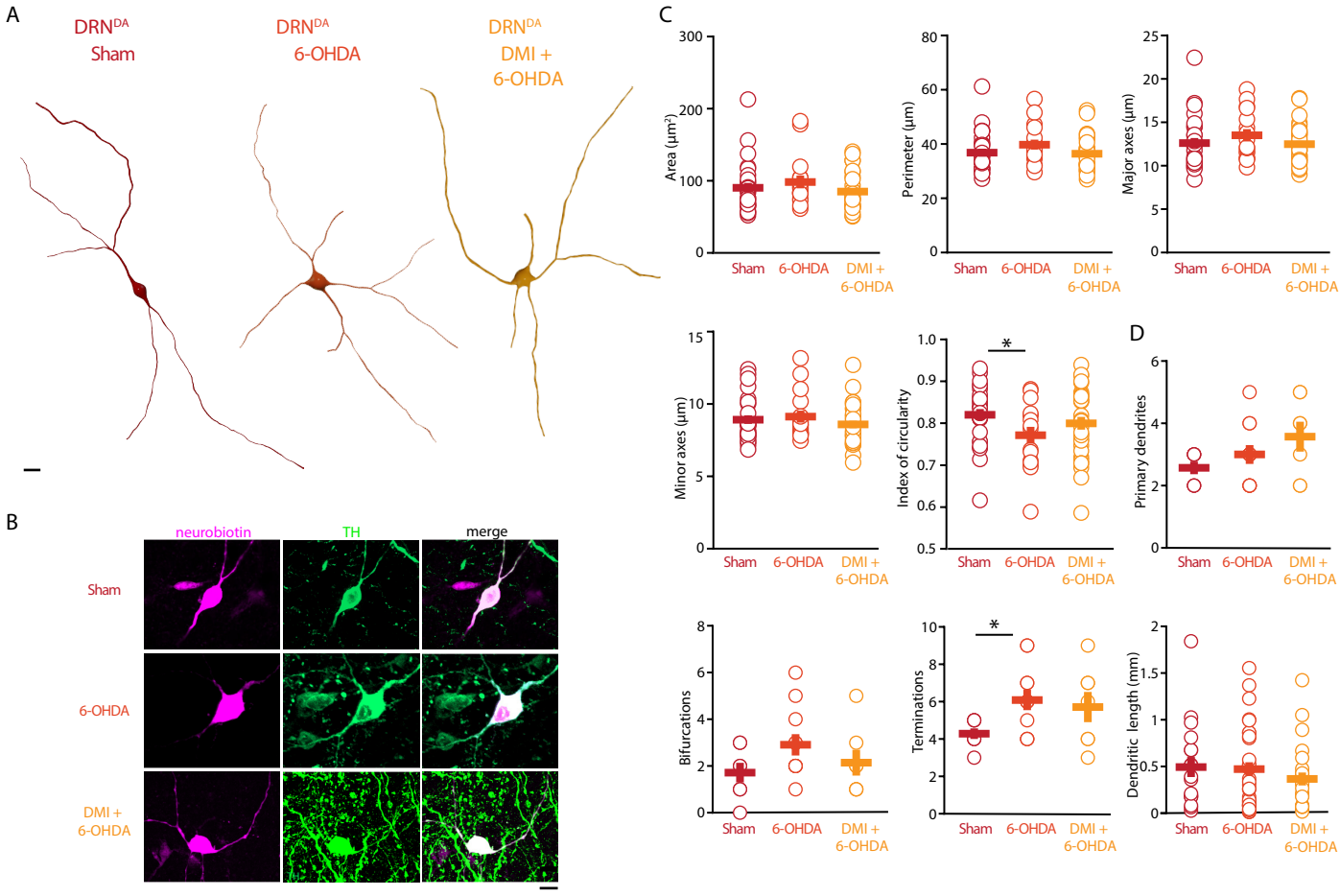
A
DRN^DA Sham
DRN^DA 6-OHDA
DRN^DA DMI + 6-OHDA
B
neurobiotin
TH
merge
Sham
6-OHDA
DMI + 6-OHDA
C
Area (µm²)
Perimeter (µm)
Major axes (µm)
Minor axes (µm)
Index of circularity
Bifurcations
Terminations
Dendritic length (mm)
Sham
6-OHDA
DMI + 6-OHDA
*
D
Primary dendrites

Fig. 6